

Research note

Experimental and Kinetic Study of CO Oxidation Over $\text{LaFe}_{1-x}\text{Cu}_x\text{O}_3$ ($x=0, 0.2, 0.4, 0.6$) Perovskite-Type Oxides

P. Rashidi Zonouz¹, M. E. Masoumi¹, A. Niaei^{1,2*}, A. Tarjomannejad²

¹ Faculty of Engineering, Tehran North Branch, Islamic Azad University, Tehran, Iran

² Department of Chemical Engineering & Petroleum, University of Tabriz, Tabriz, Iran

ARTICLE INFO

Article history:

Received: 2016-08-05

Accepted: 2017-05-30

Keywords:

CO Oxidation,

Perovskite,

$\text{LaFe}_{1-x}\text{Cu}_x\text{O}_3$,

Kinetic,

MVK Mechanism

ABSTRACT

In this paper, catalytic oxidation of CO over $\text{LaFe}_{1-x}\text{Cu}_x\text{O}_3$ ($x= 0, 0.2, 0.4, 0.6$) perovskite-type oxides was investigated. The catalysts were synthesized by sol-gel method and characterized by XRD, BET, FT-IR, H_2 -TPR, and SEM methods. The catalytic activity of catalysts was tested in catalytic oxidation of CO. XRD patterns confirmed the synthesized perovskites to be single-phase perovskite-type oxides. The synthesized perovskite catalysts show high activity in the range of reaction temperature (50 - 300 °C). The substitution of Cu in B-site of the perovskite catalysts enhanced their catalytic activity for CO oxidation. Among different synthesized perovskite catalysts, $\text{LaFe}_{0.6}\text{Cu}_{0.4}\text{O}_3$ has the highest activity: nearly complete elimination of CO was achieved at 275 °C with this catalyst. Kinetic studies for CO oxidation were performed based on power law and Mars-van Krevelen mechanisms. According to kinetic calculations, the most probable mechanism is the MKV-D (dissociative adsorption of oxygen) which can predict the experimental data with correlation coefficient of $R^2 > 0.995$.

1. Introduction

Carbon monoxide is one of the main gaseous pollutants, which is generally released from the combustion of fossil fuel in diesel engines [1]. There are many methods for removing CO including adsorption, thermal elimination, and catalytic oxidation. Catalytic oxidation of CO is proved to be one of the most efficient techniques to remove this pollutant [2, 3].

Precious metals Pt, Pd, and Rh supported on alumina and ceria have been considered as the most efficient for the control of exhaust gas

[4-7]. Due to the high cost and low stability of precious metal, considerable efforts have been paid to the utilization of perovskite catalysts [8-10].

Perovskite-type oxide catalysts are alternatives for supported noble metal catalysts. Perovskite-type oxides with the general formula ABO_3 can crystallize in cubic structure [11]. Their high activity, versatile and stable structures make them suitable catalytic materials for chemical processes. The larger A-site cation is often a rare earth,

*Corresponding author: aniaei@tabrizu.ac.ir

an alkaline earth, or an alkali metal cation, and the B-site cation is typically a smaller transition metal cation [12, 13]. Both 'A' and 'B' cations can be partially substituted, leading to substituted compounds with a general formula of $A_{1-x}A'_x B_{1-y}B'_y O_3$ [14-16].

Among the perovskite-type oxides, Iron containing perovskites has attracted more attention for CO oxidation due to their special oxygen nonstoichiometries [1]. Highly dispersed Cu^{2+} was generally regarded as an active site for CO oxidation [17-19]. So, by incorporation of copper cations into the B-site of the perovskite structure, a good performance can be achieved. However, few works reported on the effect of Cu substitution on the physicochemical properties of $LaFeO_3$ perovskite as well as their catalytic performances for CO oxidation.

Gao et al. [20] investigated $LaFeO_3$ perovskite-type catalyst for CO oxidation, and found that this catalyst has high activity in reaction temperature range. Catalytic activity of $LaMn_{1-x}Fe_xO_3$ perovskite was investigated by Zheng et al. [21] for catalytic oxidation of CO. They found that it is possible to reach a high active catalyst by appropriate x value. $LaMn_{0.4}Fe_{0.6}O_3$ has the highest activity in the studied catalysts. In another work, Yan et al. [17] investigated perovskite-type oxides with general formulation of $LaCo_{0.5}M_{0.5}O_3$ (M = Mn, Cr, Fe, Ni, Cu). $LaCo_{0.5}Mn_{0.5}O_3$ catalyst showed to be inclined towards much higher activity in CO oxidation, compared with $LaCo_{0.5}M_{0.5}O_3$ (M = Cr, Fe, Ni, Cu), due to different kinds of valence state and lattice oxygen content. Abdolrahmani et al. [22] investigated a series of $LaMn_{1-x}Cu_xO_3$ perovskite-type catalysts, with x range of 0 to 1, for CO oxidation, and found that the catalytic activity was the highest for x = 0.2. Tien et al. [18] investigated the effect of Cu

substitution in the $LaCoO_3$ perovskite structure. They found that the cobalt atom in the reduced perovskites played an important role in the dissociation of CO; however, the presence of a neighboring copper along with remnant sodium ions on the catalyst surface has remarkably affected the reactivity of cobalt for CO hydrogenation.

In this paper, effects of substitution of Fe by Cu in B-site of perovskites on chemical-physical properties and activity of catalysts were investigated. For this aim, a series of perovskite-type oxides $LaFe_{1-x}Cu_xO_3$ (x=0, 0.2, 0.4, 0.6) were prepared by sol-gel method and characterized by XRD, BET, FT-IR, H_2 -TPR, and SEM. The catalytic performances of prepared catalysts were investigated for the catalytic oxidation of CO. To investigate the kinetics of CO oxidation reaction, kinetic studies were conducted based on power law and *Mars-van Krevelen* mechanisms, and the rate constant and activation energy were evaluated under specified operating condition.

2. Materials and methods

2.1. Catalyst preparation

The solids of the general formula $LaFe_{1-x}Cu_xO_3$ (x= 0, 0.2, 0.4, 0.6) were prepared by sol-gel method. $La(NO_3)_3 \cdot 6H_2O$, $Fe(NO_3)_3 \cdot 9H_2O$, and $Cu(NO_3)_2 \cdot 3H_2O$ and Citric acid monohydrate were the starting materials. Citric acid was added over the stoichiometric amount to an aqueous solution containing La, Fe, and Cu nitrates with cation ratios La:Fe:Cu, of 1:1-x:x in order to assure complete complexation of the cations. The ratio of citric acid to nitrates was kept 0.525. The resulting mixture was evaporated at 80 °C with continuous stirring, until a sticky gel was obtained. In order to carry out gel decomposition, temperature was raised to 200 °C and, finally, the decomposed gel self-

ignited and turned into a dark powder. The gel burned at 200 °C and turned into a dark powder. Then, the powder was calcined for 5 h at 700 °C.

2.2. Characterizations

The crystal structure of the catalyst was determined by an X-ray diffractometer (D-500, SIEMENS) with a $K\alpha$ line of copper ($\lambda = 0.154$ nm). Measurements of the samples were collected in the 2θ range of 20–80 °. The BET surface area was determined by N_2 adsorption–desorption porosimetry at 77 K using a micro pore analyzer (ASAP 2010, USA). Infrared (IR) spectra were recorded with a Bruker 27 FT-IR spectrometer using the Universal ATR Accessory in the range of 4000 to 400 cm^{-1} with 4 cm^{-1} resolution. H_2 -TPR experiments were carried out using a NanoSORD NS91 apparatus. The H_2 -TPR experiments were performed on 30 mg of each catalyst placed in a U-shaped quartz reactor. Prior to each TPR run, the catalyst was degassed in a flow of 10 $\text{cm}^3 \text{min}^{-1}$ Ar at 300 °C for 1 h and cooled down to room

temperature under the same atmosphere. The sample was then reduced by 10 $\text{cm}^3 \text{min}^{-1}$ of 5.0 % H_2/Ar mixture while the temperature was raised to 950 °C with a heating rate of 10 °C/min. The morphology of the synthesized particles was observed by scanning electron microscopy using a Tescan instrument.

2.3. Catalytic activity

Catalytic activity tests for CO oxidation were carried out in a straight quartz reactor (l = 60 cm, i.d. = 0.8 cm) at atmospheric pressure and different temperatures (50 - 300 °C). 200 mg of catalyst was placed between two quartz wool plugs. The temperature was controlled using K-type thermocouple. Total flow rate of feed will be 100 $\text{cm}^3 \text{min}^{-1}$ (GHSV= 6000 h^{-1}). Feed composed of 2 % CO, 20 % O_2 , and Ar as balance. The feed and product gases were analyzed using a Shimadzu 2010 gas chromatograph (GC) equipped with a TCD detector and a HP-Molesieve (Agilent, USA) column (l = 30 m, i.d. = 0.53 mm). The schematic of the used setup is shown in Fig. 1.

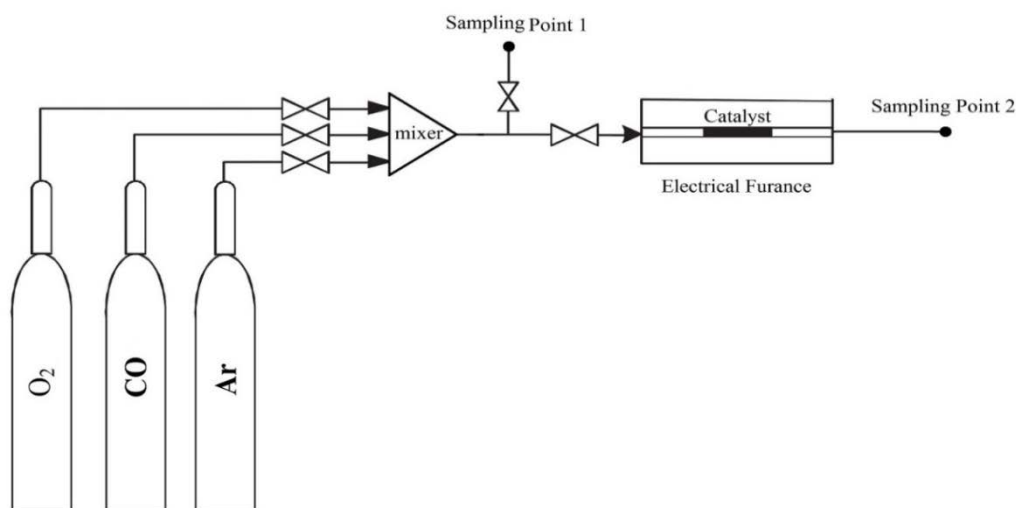


Figure 1. Schematic of experimental setup.

3. Results and discussion

3.1. Structural properties

The structure of catalysts with different

compositions was investigated using the X-ray diffraction method. XRD pattern for the catalysts is shown in Fig. 2. A comparison of

XRD patterns with the pattern of LaFeO_3 (JCPDS 37-1493) indicated that catalysts were single-phase perovskite oxides. There were no additional peaks corresponding to secondary phases or starting materials in XRD pattern of perovskites, suggesting that metals were completely dissolved in the perovskite structure. By introduction of Cu, no segregation phase was observed in the perovskites. By 2θ comparison of the catalysts' main peaks, it was revealed that the main peak of each catalyst was observed in shifted 2θ , which is the result of modifier metal insertion in the LaFeO_3 structure and change of the unit cell size.

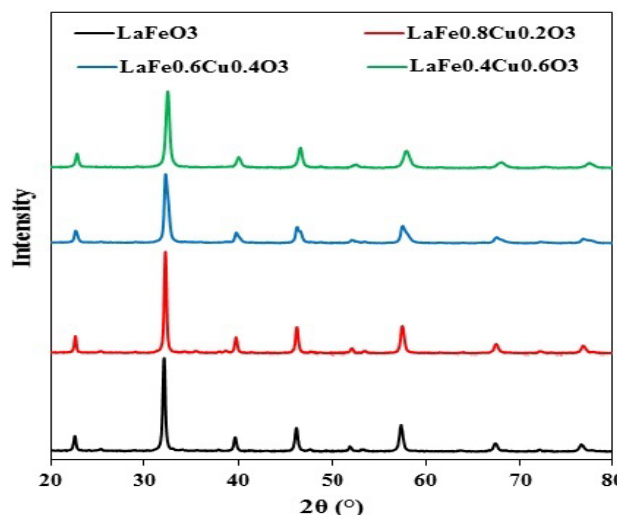


Figure 2. XRD patterns of $\text{LaFe}_{1-x}\text{Cu}_x\text{O}_3$ perovskites.

Specific surface areas of the synthesized perovskite catalysts are shown in Table 1. As

seen, the specific surface areas are in the range of $5\text{--}8\text{ m}^2/\text{g}$. From Table 1, it is evident that substitution of Fe by Cu reduces specific surface areas of perovskites.

The infrared spectra in the range of $400\text{--}4000\text{ cm}^{-1}$ of the synthesized perovskites are presented in Fig. 3. It can be seen that few organic groups are present in the synthesized perovskite catalysts. The band at 3440 cm^{-1} is assigned to O-H stretching vibration [19]. The band around 1640 cm^{-1} is assigned to C=O stretching in carboxyl or amide groups [23]. This band can also be related to the adsorption of carbon dioxide on the surface of samples. The bands around 600 cm^{-1} and 480 cm^{-1} are characteristic metal-oxygen bond [19]. These bands are assigned to Fe-O and Cu-O bonds.

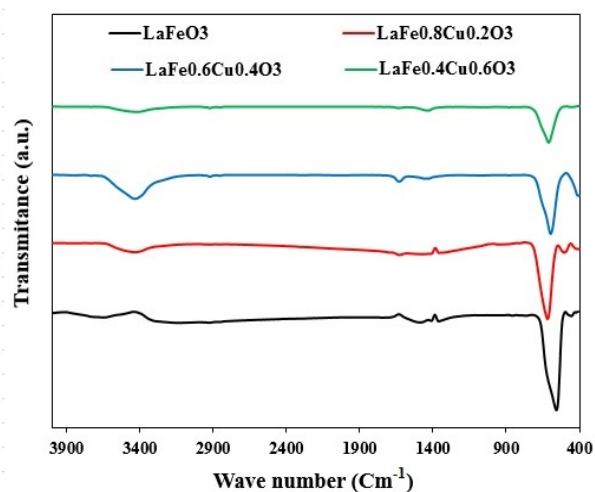


Figure 3. FT-IR spectra of $\text{LaFe}_{1-x}\text{Cu}_x\text{O}_3$ perovskites.

Table 1

T50 % and T90 % of CO conversion over synthesized perovskites.

Catalyst	BET (m^2/g)	T50% ($^{\circ}\text{C}$)	T90% ($^{\circ}\text{C}$)
LaFeO_3	8	203	245
$\text{LaFe}_{0.8}\text{Cu}_{0.2}\text{O}_3$	6	192	238
$\text{LaFe}_{0.6}\text{Cu}_{0.4}\text{O}_3$	5	177	217
$\text{LaFe}_{0.4}\text{Cu}_{0.6}\text{O}_3$	7	186	225

The H_2 -TPR studies were carried out to investigate the effect of partial substitution of Cu in B site on the reducibility of catalyst. H_2 -TPR curves of the perovskite samples are shown in Fig. 4. Regarding the H_2 -TPR profile of LaFeO_3 , there are two reduction peaks at 493 and 576 °C. The first peak corresponds to Fe^{4+} which is reduced to Fe^{3+} , and the second peak corresponds to Fe^{3+} which is reduced to Fe^{2+} [24, 25]. In the profile of $\text{LaFe}_{1-x}\text{Cu}_x\text{O}_3$ samples, one peak is observed at 275 °C, which can be attributed to the reduction of Cu^{2+} to Cu^0 and Fe^{4+} to Fe^{3+} , respectively [26, 27]. The second peak corresponds to Fe^{3+} which is reduced to Fe^{2+} .

In the TPR profiles of $\text{LaFe}_{1-x}\text{Cu}_x\text{O}_3$, the reduction temperatures of Fe^{4+} and Fe^{3+} decreased, compared to reduction temperatures of Fe^{4+} and Fe^{3+} in LaFeO_3 , and hydrogen consumption increased, revealing that the introduction of Cu promoted the reduction of iron in the perovskites. $\text{LaFe}_{1-x}\text{Cu}_x\text{O}_3$ has the highest hydrogen consumption and the lowest reduction temperature among the other synthesized catalysts.

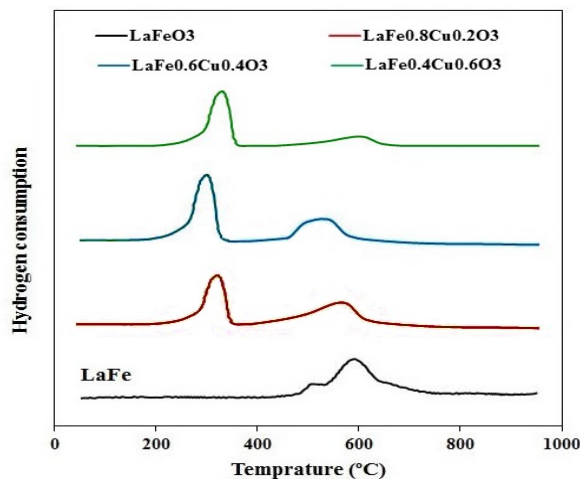


Figure 4. H_2 -TPR profiles of $\text{LaFe}_{1-x}\text{Cu}_x\text{O}_3$ perovskites.

The morphology and particle size of synthesized perovskite catalysts were investigated by scanning electron microscopy (SEM). SEM images of perovskite are shown in Fig. 5. It is observed that sol-gel method is able to produce nanosized perovskite crystal close to 100 nm. All catalysts are formed by large agglomerated/sintered particles with random shapes. It is observed that the particle sizes are different for the samples.

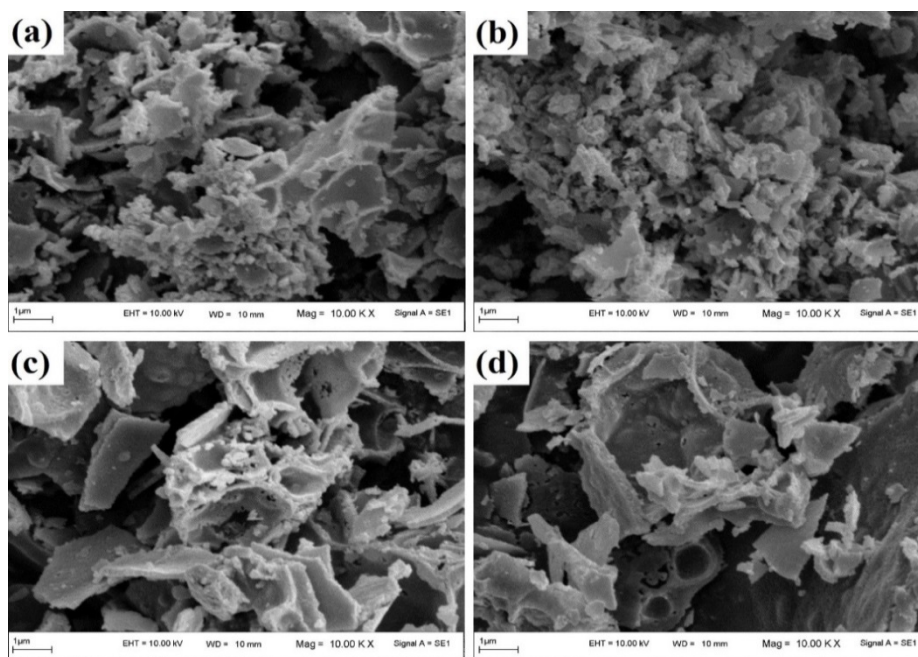


Figure 5. SEM images of $\text{LaFe}_{1-x}\text{Cu}_x\text{O}_3$ perovskites: (a) $x=0$, (b) $x=0.2$, (c) $x=0.4$, and (d) $x=0.6$.

3.2. Activity of catalysts

Results from the catalytic activity tests in CO oxidation are shown in Fig. 6. The temperatures for 50 % and 90 % conversions of CO (T50 % and T90 %) on $\text{LaFe}_{1-x}\text{Cu}_x\text{O}_3$ are listed in Table 1. By considering T50 % and T90 % of CO conversions as a criterion of activity, the following order was observed for performance of catalysts: $\text{LaFeO}_3 < \text{LaFe}_{0.8}\text{Cu}_{0.2}\text{O}_3 < \text{LaFe}_{0.4}\text{Cu}_{0.6}\text{O}_3 < \text{LaFe}_{0.6}\text{Cu}_{0.4}\text{O}_3$. Obviously, partial substituting of Fe by Cu in B-site has large effect on catalyst activity. Therefore, among the studied $\text{LaFe}_{1-x}\text{Cu}_x\text{O}_3$ perovskites, $\text{LaFe}_{0.6}\text{Cu}_{0.4}\text{O}_3$ was found to be the most active one.

In addition, the stability of catalysts was studied at 225 °C for 20 h. The result of the stability of catalysts is shown in Fig. 7. The

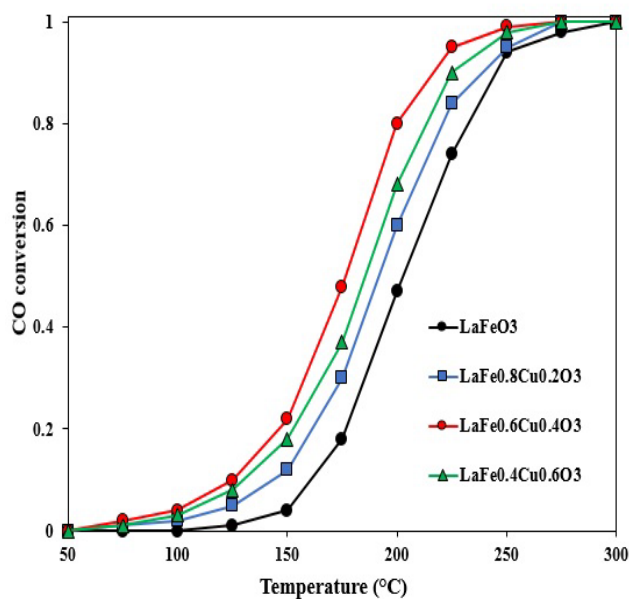


Figure 6. Conversion profile of CO as a function of temperature over synthesized perovskites.

Table 2 shows the comparison between the obtained results in this work and other literature. The results show that the best catalyst in this work, compared with other catalysts, has a good performance.

catalysts showed good stability; after 20 hours, the CO conversion for all catalysts is not changed.

Catalytic activity of perovskites for CO oxidation depends on reducibility of transition metal cations, oxygen vacancy concentration, and specific surface area. Substitution of Fe by Cu in the perovskite reduced the reduction temperature of iron and increased the reducibility of perovskites [28]. Substitution of cations in the perovskite modifies the surface structure of catalyst by increasing the oxygen valences in the surface regions, resulting in high activity. Based on BET results and catalytic performance for synthesized perovskites, no direct relationship was observed between activity and specific surface area of perovskites in catalytic oxidation of CO.

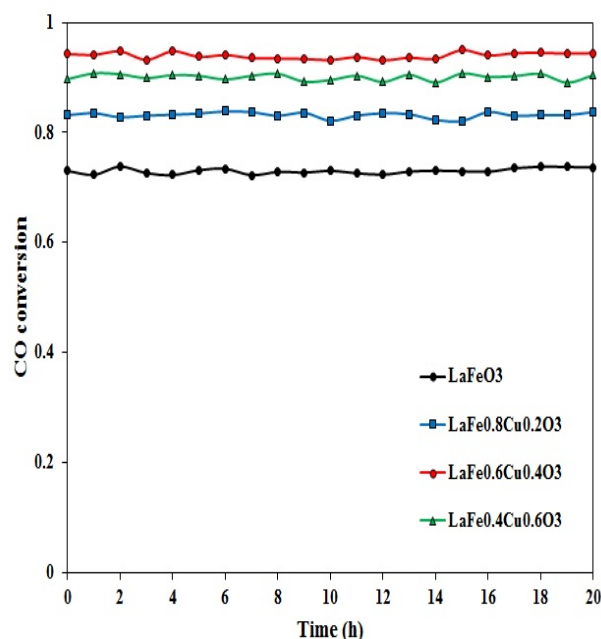


Figure 7. Stability of perovskite catalysts.

3.3. Kinetic modeling

In order to extend the analysis of the reasons further for the different behavior of $\text{LaFe}_{1-x}\text{Cu}_x\text{O}_3$, the investigation of the kinetics and mechanism was carried out. Power law

kinetic models (PWL) and two Mars–van Krevelen models were fitted with the experimental data. The Mars–van Krevelen models (MVK) suppose non-dissociative or dissociative adsorptions of the oxygen.

Table 2

Comparison of the catalytic activities of LaFe_{0.6}Cu_{0.4}O₃ catalyst with other catalysts from literature.

Catalyst	CO %	O ₂ %	Flow rate (ml/min)	Conversion at 250 °C
LaFe _{0.6} Cu _{0.4} O ₃ This work	2	20	100	96
LaFeO ₃ Gao et al. [20]	1	20	100	84
LaFe _{0.6} Mn _{0.4} O ₃ Zheng et al. [21]	1	20	20	15
LaCo _{0.5} Mn _{0.5} O ₃ Yan et al. [17]	1.5	20	550	93
LaMn _{0.6} Cu _{0.4} O ₃ Abdolrahmani et al. [22]	2	20	50	70
La _{0.5} Sr _{0.5} MnO ₃ Jaenicke et al. [29]	8	4	100	48
LaCoO ₃ Femina et al. [30]	6.8	17.6	440	96

PLW model: Kinetic equation for the power law model (PLM) will be derived as in equation (1):

$$r = kC_{CO}^{n_1}C_{O_2}^{m_1} \quad (1)$$

k is expressed as in equation (2):

$$k = k_0 \exp\left(\frac{-E_a}{RT}\right) \quad (2)$$

MVK-ND: First, MVK model hypothesized non-dissociative adsorption of oxygen (MVK-ND). In this case, reaction steps are based on equations (3) and (4), and the rate equation is derived from equation (5).



$$r = \frac{k_{red}k_{ox}P_{CO}P_{Ox}}{\gamma k_{red}k_{CO} + k_{ox}P_{Ox}} \quad \gamma = \frac{1}{2} \quad (5)$$

where S is a surface active site.

MVK-D: Second, MVK model hypothesized dissociative adsorption of oxygen (MVK-D). In this case, reaction steps are based on equations (6) and (7), and the rate equation will be derived from equation (8).



$$r = \frac{k_{red}k_{ox}P_{CO}P_{Ox}^{1/2}}{\gamma k_{red}k_{CO} + k_{ox}P_{Ox}^{1/2}} \quad \gamma = \frac{1}{2} \quad (8)$$

k_{red} and k_{ox} are expressed in equations (9) and (10), respectively:

$$k_{red} = k_{0,red} \exp\left(\frac{-E_{a,red}}{RT}\right) \quad (9)$$

$$K_{ox} = k_{0,CO} \exp\left(\frac{E_{a,ox}}{RT}\right) \quad (10)$$

Regarding the specifics in deriving the rate equations for MVK models, detailed description is given in the literature [31, 32].

The catalytic bed, which has been modeled as a one-dimensional system, is treated as a plug flow reactor. The mass balance equations in the steady state condition are according to equation (11).

$$\frac{dc_i}{dz} = \frac{1}{u_{eff}} \sum_j v_j r \quad i = CO \text{ and } O_2 \quad (11)$$

For fitting the kinetic parameters, continuity equations for CO and oxygen in the steady state condition are solved numerically. These simulations were created by writing computer codes in MATLAB™ 7.2 software. A non-linear least square algorithm minimizes

average absolute derivation between the experimental and calculated data.

Further evaluation of the efficiency and accuracy of the proposed models was performed by utilizing some statistical parameters. These parameters included average absolute deviation (AAD %) and correlation coefficient (R^2), which are represented as in equations (12) and (13), respectively [33, 34].

$$AAD \% = \frac{100}{N} \sum_{i=1}^N |x_i^{exp} - x_i^{cal}| \quad (12)$$

$$R^2 = \frac{\sum_{i=1}^N (x_i^{exp} - \bar{x})^2 - \sum_{i=1}^N (x_i^{exp} - x_i^{cal})^2}{\sum_{i=1}^N (x_i^{exp} - \bar{x})^2} \quad (13)$$

where N is the number of data points, x_i^{exp} is the i^{th} experimental conversion, x_i^{cal} is the i^{th} calculated conversion, and \bar{x} is the average value of experimental conversion data.

The estimated kinetic parameters, the

correlation coefficients (R^2), and average absolute derivation (AAD %) for various models are listed in Table 3. These parameters are calculated based on differences between experimental and calculated data for each catalyst. Comparisons between experimental and modelling results for CO conversion for all models are shown in Fig. 8.

Based on results, PLW model can predict the experimental data with good accuracy; however, this model does not give any information about the activation energy. Based on the results, MVK-D [$\text{CO} + \text{S} \rightarrow (\text{CO})\text{S}$; $\text{O}_2 + 2\text{S} \rightarrow 2(\text{O})\text{S}$] model was observed to provide a consistent mechanism for the studied catalysts. Therefore, MKK-D mechanism is has highre possibility to work than MVK-ND mechanism. It is clear from Fig. 6 that there is good agreement between experimental and calculated data for MVK-D model.

Table 3

Kinetics parameters for applied Mars–van Krevelen and power law models.

PLW model						
	AAD %	R^2	K_0	E_a	m	n
LaFeO ₃	1.65	0.9941	9.37E+09	76800	0.51	0.43
LaFe _{0.8} Cu _{0.2} O ₃	2.65	0.9931	4.54E+09	72600	0.46	0.39
LaFe _{0.6} Cu _{0.4} O ₃	2.23	0.9945	3.37E+09	69300	0.42	0.36
LaFe _{0.4} Cu _{0.6} O ₃	2.62	0.9921	4.01E+09	71000	0.43	0.38
MVK-ND						
	AAD %	R^2	$k_{0,red}$	$k_{0,ox}$	$E_{a,red}$	$E_{a,ox}$
LaFeO ₃	2.22	0.9883	7.76E+09	6.86E+10	44.3	89.8
LaFe _{0.8} Cu _{0.2} O ₃	3.36	0.9834	3.23E+09	2.72E+10	41.5	83.4
LaFe _{0.6} Cu _{0.4} O ₃	2.89	0.9912	2.39E+09	3.72E+09	38.2	75.1
LaFe _{0.4} Cu _{0.6} O ₃	2.52	0.991	2.57E+09	3.98E+09	39.9	76.4
MVK-D						
	AAD %	R^2	$k_{0,red}$	$k_{0,ox}$	$E_{a,red}$	$E_{a,ox}$
LaFeO ₃	1.81	0.9967	1.92E+06	9.77E+06	29.6	58.7
LaFe _{0.8} Cu _{0.2} O ₃	0.96	0.9985	1.08E+06	7.31E+06	27.2	56.1
LaFe _{0.6} Cu _{0.4} O ₃	0.95	0.9989	8.16E+05	6.91E+06	24.6	53.6
LaFe _{0.4} Cu _{0.6} O ₃	1.07	0.9985	9.18E+05	7.05E+06	26.3	54.5

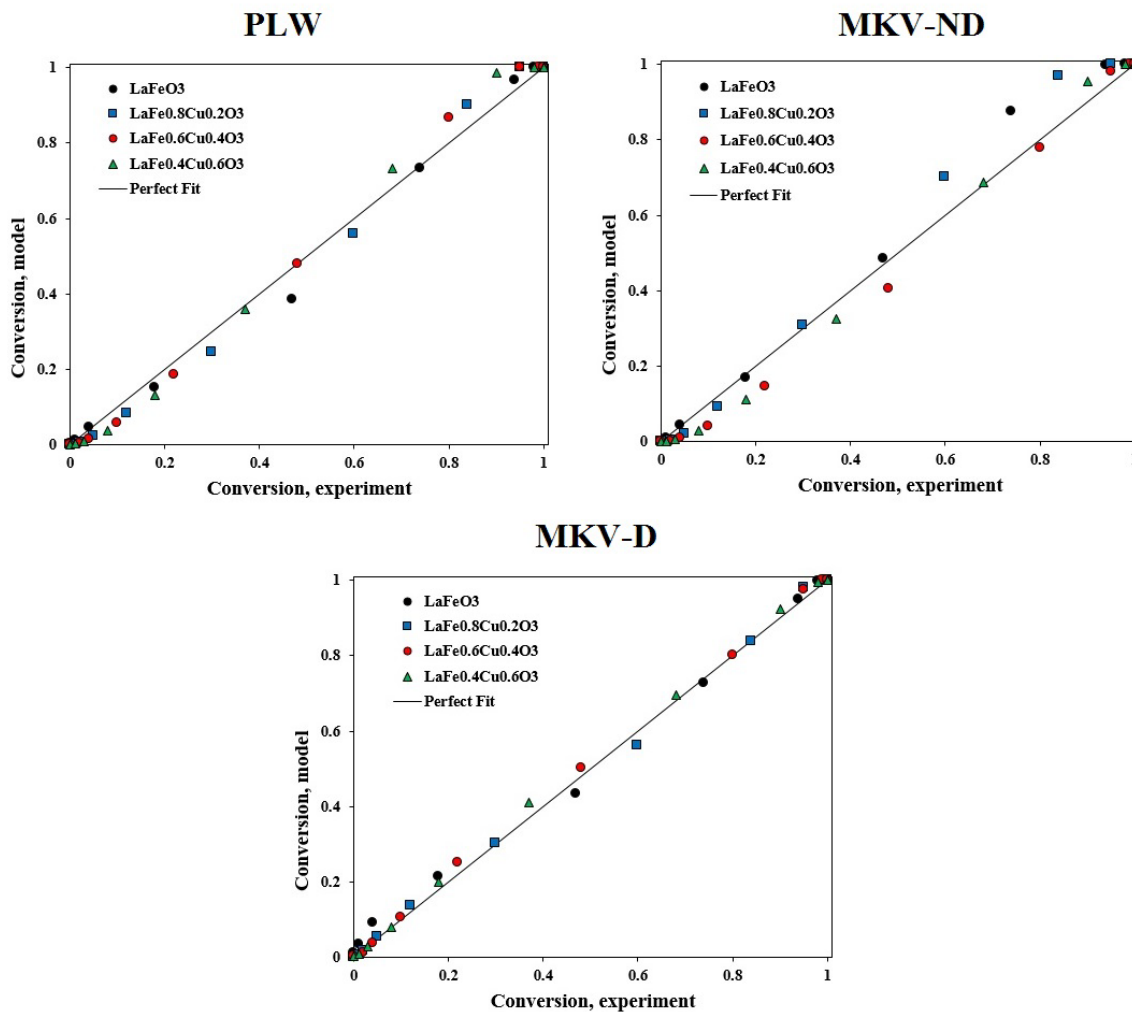


Figure 8. Comparison between experimental and simulated data for various models.

Substitution of iron by copper reduces the apparent activation energy for CO oxidation. The lower apparent activation energy coincides with the observed increase in catalytic activity. $\text{LaFe}_{0.6}\text{Cu}_{0.4}\text{O}_3$ which has the lowest activation energy ($E_{a,\text{red}}=24.6$ kJ/mol and $E_{a,\text{ox}}=53.6$ kJ/mol), was also found to be the most active catalyst in the synthesized perovskites, and LaFeO_3 had the highest activation energy ($E_{a,\text{red}}=29.6$ kJ/mol and $E_{a,\text{ox}}=58.7$ kJ/mol). The values of activation energies do not show sensible changes with B cations and x value. Chan et al. [35] found the apparent activation energy of $\text{La}_{1-x}\text{Sr}_x\text{MnO}_3$ perovskites between 48.3 and 66 kJ/kmol. Wang et al. [36] calculated activation energy of LaSrNiO_4 to be equal to

49.3 kJ/mol. Variation of activation energy with introduction of cations in B site is small. These values are compared satisfactorily with the values calculated in this work.

4. Conclusions

Catalytic performance of sol-gel synthesized $\text{LaFe}_{1-x}\text{Cu}_x\text{O}_3$ ($x= 0, 0.2, 0.4,$ and 0.6) perovskite catalysts was evaluated in the catalytic oxidation of CO. The XRD results confirmed that the sol-gel method produced pure perovskite structure. SEM results also revealed that all catalysts were formed by large agglomerated/sintered particles with a random shape. Among the studied $\text{LaFe}_{1-x}\text{Cu}_x\text{O}_3$ perovskites, $\text{LaFe}_{0.6}\text{Cu}_{0.4}\text{O}_3$ was found to be the most active catalyst. Substitution of

Fe by Cu in the perovskite reduced the reduction temperatures of Fe^{4+} and Fe^{3+} , compared to reduction temperatures of Fe^{4+} and Fe^{3+} in LaFeO_3 ; hydrogen consumption was increased, which resulted in high activity. The catalysts showed good stability; after 20 hours, the CO conversion for all catalysts did not change. Based on power law and Mars-van Krevelen mechanisms, kinetic studies were performed for CO oxidation, where kinetic parameters (including k_0 , E_1 , $k_{0,\text{CO}}$, ΔH_{CO} , $k_{0,\text{OX}}$ and ΔH_{OX}) were estimated. The study showed the MKV-D mechanism [$\text{CO} + \text{S} \rightarrow (\text{VOC})\text{S}$; $\text{O}_2 + 2\text{S} \rightarrow 2(\text{O})\text{S}$] as being more probable than other mechanisms. These findings indicated that the proposed model could be successfully used to predict catalyst activity in CO oxidation.

References

- [1] Tarjomannejad, A., Niaei, A., Farzi, A., Salari, D. and Zonouz, P. R., "Catalytic oxidation of CO over $\text{LaMn}_{1-x}\text{B}_x\text{O}_3$ (B= Cu, Fe) Perovskite-type oxides", *Catalysis Letters*, **148**, 1544 (2016).
- [2] Ladas, S., Poppa, H. and Boudart, M., "The adsorption and catalytic oxidation of carbon monoxide on evaporated palladium particles", *Surface Science*, **102**, 151 (1981).
- [3] Tang, X., Hao, J. and Li, J., "Complete oxidation of methane on $\text{Co}_3\text{O}_4\text{-SnO}_2$ catalysts", *Frontiers of Environmental Science & Engineering in China*, **3**, 265 (2009).
- [4] Shelef, M. and Graham, G., "Why rhodium in automotive three-way catalysts?", *Catalysis Reviews*, **36**, 433 (1994).
- [5] Armor, J. N., "Environmental catalysis", *Applied Catalysis B: Environmental*, **1**, 221 (1992).
- [6] Taylor, K. C., "Nitric oxide catalysis in automotive exhaust systems", *Catalysis Reviews-Science and Engineering*, **35**, 457 (1993).
- [7] Hungria, A., Browning, N., Erni, R., Fernández-García, M., Conesa, J., Pérez-Omil, J. and Martínez-Arias, A., "The effect of Ni in Pd-Ni/(Ce, Zr) $\text{O}_x/\text{Al}_2\text{O}_3$ catalysts used for stoichiometric CO and NO elimination. Part 1: Nanoscopic characterization of the catalysts", *Journal of Catalysis*, **235**, 251 (2005).
- [8] Zhu, J., Zhao, Z., Xiao, D., Li, J., Yang, X. and Wu, Y., "Study of $\text{La}_{2-x}\text{Sr}_x\text{CuO}_4$ (x= 0.0, 0.5, 1.0) catalysts for NO + CO reaction from the measurements of O_2 -TPD, H_2 -TPR and cyclic voltammetry", *Journal of Molecular Catalysis, A: Chemical*, **238**, 35 (2005).
- [9] Viswanathan, B., "CO oxidation and NO reduction on perovskite oxides", *Catalysis Reviews*, **34**, 337 (1992).
- [10] Tou, A., Einaga, H. and Teraoka, Y., "Effect of co-deposition of LaFeO_3 on the catalytic properties of Pd on Al_2O_3 support for CO-O_2 and NO-CO reactions", *Reaction Kinetics, Mechanisms and Catalysis*, **114**, 409 (2015).
- [11] Tanaka, H. and Misono, M., "Advances in designing perovskite catalysts", *Current Opinion in Solid State and Materials Science*, **5**, 381 (2001).
- [12] Keav, S., Matam, S. K., Ferri, D. and Weidenkaff, A., "Structured Perovskite-based catalysts and their application as three-way catalytic converters: A review", *Catalysts*, **4**, 226 (2014).
- [13] Izadkhah, B., Niaei, A., Salari, D., Hosseini, S., Hosseini, S. A. and Tarjomannejad, A., "Catalytic removal of CO and NOx using sol-gel synthesized

- $\text{LaB}_{0.5}\text{Co}_{0.5}\text{O}_3$ (B= Cr, Mn and Cu) and $\text{LaMn}_x\text{Co}_{1-x}\text{O}_3$ nano-perovskites”, *Korean Journal of Chemical Engineering*, **33**, 1192 (2016).
- [14] Buciuman, F.-C., Joubert, E., Menezes, J.-C. and Barbier, J., “Catalytic properties of $\text{La}_{0.8}\text{A}_{0.2}\text{MnO}_3$ (A= Sr, Ba, K, Cs) and $\text{LaMn}_{0.8}\text{B}_{0.2}\text{O}_3$ (B= Ni, Zn, Cu) perovskites: 2. Reduction of nitrogen oxides in the presence of oxygen”, *Applied Catalysis B: Environmental*, **35**, 149 (2001).
- [15] Wu, X., Xu, L. and Weng, D., “The NO selective reduction on the $\text{La}_{1-x}\text{Sr}_x\text{MnO}_3$ catalysts”, *Catalysis Today*, **90**, 199 (2004).
- [16] Zonouz, P. R., Niaei, A. and Tarjomannejad, A., “Modeling and optimization of toluene oxidation over perovskite-type nanocatalysts using a hybrid artificial neural network-genetic algorithm method”, *Journal of the Taiwan Institute of Chemical Engineers*, **65**, 276 (2016).
- [17] Yan, X., Huang, Q., Li, B., Xu, X., Chen, Y., Zhu, S. and Shen, S., “Catalytic performance of $\text{LaCo}_{0.5}\text{M}_{0.5}\text{O}_3$ (M= Mn, Cr, Fe, Ni, Cu) perovskite-type oxides and $\text{LaCo}_{0.5}\text{Mn}_{0.5}\text{O}_3$ supported on cordierite for CO oxidation”, *Journal of Industrial and Engineering Chemistry*, **19**, 561 (2013).
- [18] Tien-Thao, N., Alamdari, H. and Kaliaguine, S., “Characterization and reactivity of nanoscale La (Co, Cu) O_3 perovskite catalyst precursors for CO hydrogenation”, *Journal of Solid State Chemistry*, **181**, 2006 (2008).
- [19] Zonouz, P. R., Niaei, A. and Tarjomannejad, A., “Kinetic modeling of CO oxidation over $\text{La}_{1-x}\text{A}_x\text{Mn}_{0.6}\text{Cu}_{0.4}\text{O}_3$ (A= Sr and Ce) nano perovskite-type mixed oxides”, *International Journal of Environmental Science and Technology*, **13**, 1665 (2016).
- [20] Gao, B., Deng, J., Liu, Y., Zhao, Z., Li, X., Wang, Y. and Dai, H., “Mesoporous LaFeO_3 catalysts for the oxidation of toluene and carbon monoxide”, *Chinese Journal of Catalysis*, **34**, 2223 (2013).
- [21] Zheng, S., Hua, Q., Gu, W. and Liu, B., “Catalytic oxidation of CO on $\text{LaMn}_{1-x}\text{Fe}_x\text{O}_3$ perovskites solid solution”, *Journal of Molecular Catalysis, A: Chemical*, **391**, 7 (2014).
- [22] Abdolrahmani, M., Parvari, M. and Habibpoor, M., “Effect of copper substitution and preparation methods on $\text{LaMnO}_{3\pm\delta}$ structure and catalysis of methane combustion and CO oxidation”, *Chinese Journal of Catalysis*, **31**, 394 (2010).
- [23] Megha, U., Shijina, K. and Varghese, G., “Nanosized $\text{LaCo}_{0.6}\text{Fe}_{0.4}\text{O}_3$ perovskites synthesized by citrate sol gel auto combustion method”, *Processing and Application of Ceramics*, **8**, 87 (2014).
- [24] Tarjomannejad, A., Farzi, A., Gómez, M. J. I., Niaei, A., Salari, D. and Albaladejo-Fuentes, V., “Catalytic reduction of NO by CO over $\text{LaMn}_{1-x}\text{Fe}_x\text{O}_3$ and $\text{La}_{0.8}\text{A}_{0.2}\text{Mn}_{0.3}\text{Fe}_{0.7}\text{O}_3$ (A= Sr, Cs, Ba, Ce) Perovskite catalysts”, *Catalysis Letters*, **146**, 2330 (2016).
- [25] Tarjomannejad, A., Farzi, A., Niaei, A. and Salari, D., “An experimental and kinetic study of toluene oxidation over $\text{LaMn}_{1-x}\text{B}_x\text{O}_3$ and $\text{La}_{0.8}\text{A}_{0.2}\text{Mn}_{0.3}\text{B}_{0.7}\text{O}_3$ (A= Sr, Ce and B= Cu, Fe) nano-perovskite catalysts”, *Korean Journal of Chemical Engineering*, **33**, 2628 (2016).
- [26] Abdolrahmani, M., Parvari, M. and Habibpoor, M., “Effect of copper

- substitution and preparation methods on the $\text{LaMnO}_{3\pm\delta}$ structure and catalysis of methane combustion and CO oxidation”, *Chinese Journal of Catalysis*, **31**, 394 (2010).
- [27] Meiqing, S., Zhen, Z., Jiahao, C., Yugeng, S., Jun, W. and Xinquan, W., “Effects of calcium substitute in LaMnO_3 perovskites for NO catalytic oxidation”, *Journal of Rare Earths*, **31**, 119 (2013).
- [28] Yu, Z., Gao, L., Yuan, S. and Wu, Y., “Solid defect structure and catalytic activity of perovskite-type catalysts $\text{La}_{1-x}\text{SrNiO}_3$ -[small lambda] and $\text{La}_{1-1.333}\text{ThNiO}_3$ -[small lambda]”, *Journal of the Chemical Society, Faraday Transactions*, **88**, 3245 (1992).
- [29] Jaenicke, S., Chuah, G. and Lee, J., “Catalytic CO oxidation over manganese-containing perovskites”, *In Fourth Symposium on Our Environment, Springer*, 131 (1991).
- [30] Femina, P. and Sanjay, P., “ LaCoO_3 perovskite catalysts for the environmental application of Auto motive CO oxidation”, *Research Journal of Recent Sciences*, **1**, 178 (2012).
- [31] Vannice, M. A., “An analysis of the Mars–van Krevelen rate expression”, *Catalysis Today*, **123**, 18 (2007).
- [32] Doornkamp, C. and Ponec, V., “The universal character of the Mars and Van Krevelen mechanism”, *Journal of Molecular Catalysis, A: Chemical*, **162**, 19 (2000).
- [33] Tarjomannejad, A., “Prediction of the liquid vapor pressure using the artificial neural network-group contribution method”, *Iran. J. Chem. Chem. Eng.*, **34**, 97 (2015).
- [34] Farzi, A. and Tarjomannejad, A., “Prediction of phase equilibria in binary systems containing acetone using artificial neural network”, *International Journal of Scientific & Engineering Research*, **9**, 358 (2015).
- [35] Chan, K., Ma, J., Jaenicke, S., Chuah, G. and Lee, J., “Catalytic carbon monoxide oxidation over strontium, cerium and copper-substituted lanthanum manganates and cobaltates”, *Applied Catalysis, A: General*, **107**, 201 (1994).
- [36] Wang, K. and Zhong, P., “A kinetic study of CO oxidation over the perovskite-like oxide LaSrNiO_4 ”, *Journal of the Serbian Chemical Society*, **75**, 249 (2010).